https://doi.org/10.3311/ECCOMASMBD2021-114

Synchronous Contact/Impact Events Modelling With A Smooth-Based Approach

Raúl Gismeros Moreno, Eduardo Corral Abad, Jesús Meneses Alonso, María Jesús Gómez García, Cristina Castejón Sisamón

MAQLAB Research Group, Department of Mechanical Engineering
Universidad Carlos III de Madrid
Avenida de la Universidad 30, 28911 Leganés, Spain
[rgismero, ecorral, meneses, mjggarci, castejon]@ing.uc3m.es

ABSTRACT

This work focuses its scope on the smooth contact approach and its management of multiple contact events, proposing several models developed under this methodology and discussing the main issues that have arisen when designing, modelling, and verifying them. The main purpose of this paper is to provide a reference to those researchers that work with smooth methods in the context of multibody dynamics of how to deal with them. Among the models presented, there are some engineering-focused ones, whereas the readers can also find some more practical, day-to-day examples.

Keywords: Contact phenomena, Contact detection, Smooth approaches, Multiple-simultaneous impact systems, Multibody System dynamics, Error containment methods.

1. INTRODUCTION

Contact forces and impact events, which are present in almost all fields of engineering [1]–[3], provokes the appearance of harmful phenomena in mechanical systems (vibrations [4], wave propagation [5], fatigue [6], wear [7], crack [8] and so on). In impact events, sudden changes take place, in which the conditions of the mechanical system vary in very short times. This causes the appearance of great magnitude forces, energy dissipation processes and both velocities and accelerations discontinuities, among other issues. Contact/impact events are difficult to model and pose a challenge for the engineers due to the large number of variables that must be taken into account: contacting surfaces geometry, material properties, inclusion of friction phenomena, multiple-simultaneous impacts, …

There are two main approaches when modelling contact events: the non-smooth approach and the models based on contact forces. Each one has a distinct set of advantages and limitations [9]: non-smooth methods are known for considering bodies as rigids solids and their computational efficiency. However, some of these methods pose several issues when dealing with friction phenomena or multiple-simultaneous impact scenarios. On the other hand, models based on contact forces are continuous functions of the relative penetration (and its temporal derivative) of the contacting bodies, which are supposed to be deformable. Their main benefit is that there is no need to define unilateral restrictions. Nonetheless, the proper, accurate choice of the parameters of the definitions of the forces, as well as the right detection of the initial instant of contact [10], that makes the computing time to increase dramatically on certain occasions, are their most distinctive drawbacks.

This paper focuses on the latter, collecting the expertise of several previous works based on this approach. Some of the most typical issues related to these methods are commented through a set of simple, day-to-day models. Then, different alternatives to overcome them are proposed.

The manuscript is structured as follows: in Section 2 the main contact detection algorithms

https://doi.org/10.3311/ECCOMASMBD2021-114

associated to the described models are presented, along with some of the most used contact force models. In Sections 3, 4 and 5 the three models are introduced and outlined, underlining their most distinctive features along with some of the results obtained and the issues arisen during the tests. The main conclusions are drawn in Section 6.

2. CONTACT DETECTION ALGORITHMS AND CONTACT FORCE MODELS

In this section, some detection algorithms for the most basis contact interactions are presented and developed. Subsequently, the contact force models used in the models later described are introduced and detailed.

2.1. Contact detection algorithms

2.1.1. Sphere-sphere interaction

A system consisting of two spheres *u* and *v* with radii R_u and R_v, respectively, coming into contact is presented in Figure 1. Two different interactions can take place, according to the arrangement of the bodies: an external contact (Figure 1 (a)) or an internal one (Figure 1 (b)).

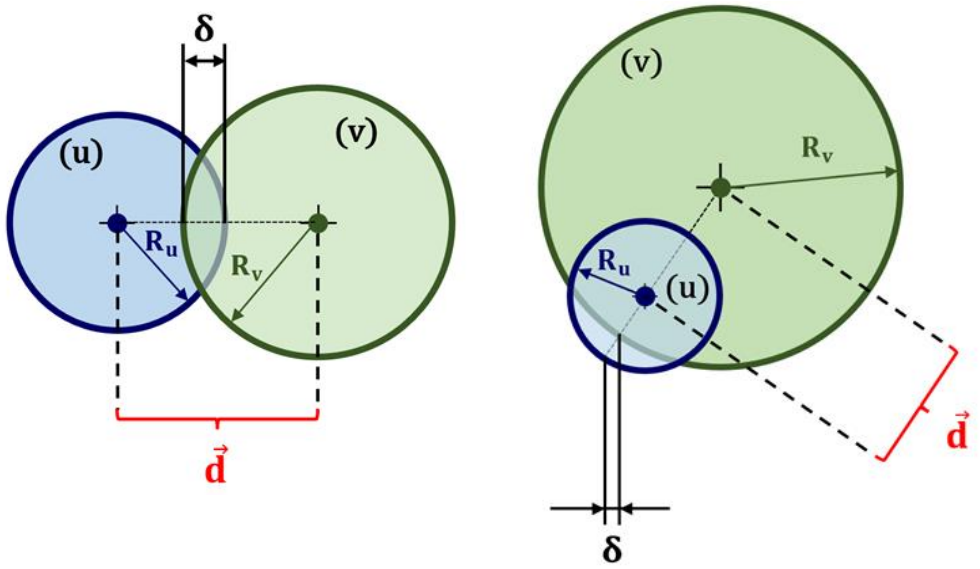

(a) (b)

Figure 1. Sphere-sphere contact interaction.

The algorithm for calculating the relative penetration between the bodies varies minimally between both cases. For an external contact, the expression that defines penetration, δ, is

$$\delta = R_u + R_v - \left\|\vec{d}\right\| \tag{1}$$

Whereas the value of the indentation in an internal interaction is given by the following equation

$$\delta = R_u + R_v + \left\|\vec{d}\right\| \tag{2}$$

However, in this last case, the value of the largest radius is introduced with negative sign. For both interactions, if δ is negative, no contact will be happening, being the initial instant of contact when $\delta = 0$.

2.1.2. Sphere-plane interaction

Given the system shown in Figure 2 formed by a sphere *u* (its centre being on point C, with radius R) and an infinite plane *v* (its mass centre being on P), the implicit function or general equation is defined

$$a \cdot x + b \cdot y + c \cdot z + d = 0 \tag{3}$$

https://doi.org/10.3311/ECCOMASMBD2021-114

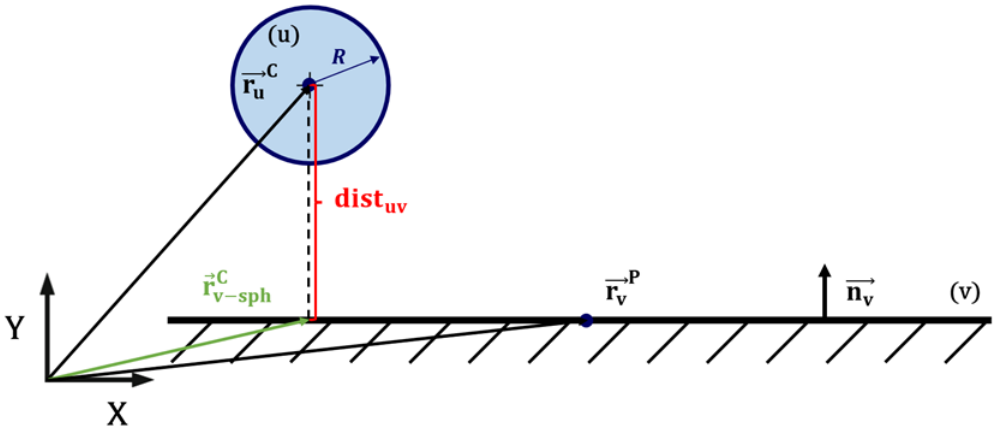

Figure 2. Sphere-plane contact interaction.

where *a*, *b* and *c* denote the components of the vector normal to the plane in the XYZ global frame, respectively. Using the coordinates of the plane mass centre, the value of parameter *d* is obtained

$$d = -a \cdot r_x^P - b \cdot r_y^P - c \cdot r_z^P \tag{4}$$

With d the distance from the centre of the sphere to the plane, $dist_{uv}$, can be calculated

$$dist_{uv} = \vec{n}_v \cdot \vec{r}_u^C + d \tag{5}$$

The projection of the mass centre of the sphere on plane *v*, $\vec{r}_{v-sph}^C$ is then defined

$$\vec{r}_{v-sph}^C = \vec{r}_u^C - dist_{uv} \cdot \vec{n}_v \tag{6}$$

This projection must be changed into local-frame plane coordinates when obtaining the value of the relative contact velocity

$$\vec{s}_{v-sph}^C = A_v^{-1} \cdot (\vec{r}_{v-sph}^C - \vec{r}_v^P) \tag{7}$$

Once the $dist_{uv}$ is calculated, δ can be derived

$$\delta = R - dist_{uv} \tag{8}$$

Negative values of penetration indicate that there is no contact happening between the sphere and the plane. The initial instant of contact takes place when $\delta = 0$.

A set of more complex interaction can be derived from these simple algorithms, as shown in Figure 3 [11].

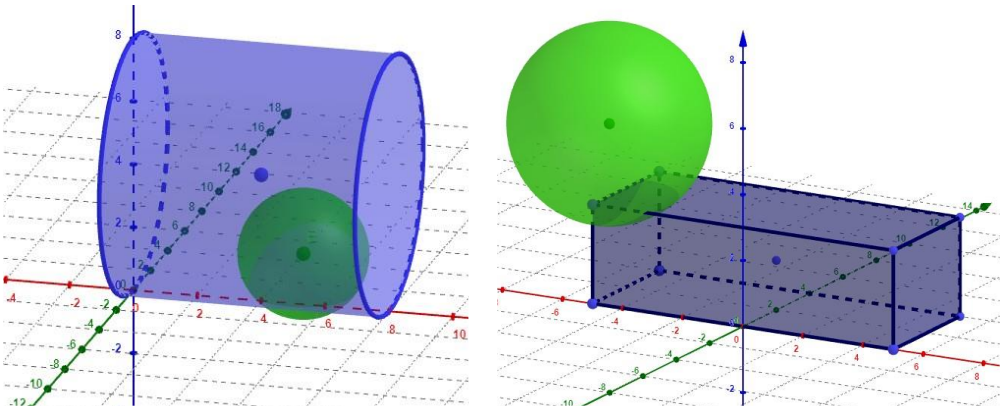

(a) (b)

Figure 3. Complex contact interactions derived from the ones introduced above [11]: (a) Sphere-cylinder; (b) Sphere-parallelepiped.

https://doi.org/10.3311/ECCOMASMBD2021-114

2.2. Contact forces models

Once the contact condition is met, a suitable constitutive law is required to obtain the value of the contact force. The interested reader can find a wide variety of works that collect a reasonably large number of contact force models [9], [12], [13], most of them proposed in the last decades. The models developed in this work make use of some of the most widely used and well-known contact laws.

The overall integrity of the model and an accurate contact detection are pursued during the early stages of the design and development of a model. For this purpose, Hertzian contact model proves to be the right choice, which defines force as a function of the relative penetration between the contacting bodies:

$$F_N = K \cdot \delta^n \tag{9}$$

where K is the contact stiffness parameter and n is an exponent that quantifies the degree of nonlinearity of the force-indentation relation [9]. The definition of the K varies depending on the geometries of the bodies involved in the contact process. Exponent n usually takes a value of 3/2, according to the work by Hertz, who assumed a parabolic distribution of the stresses in the contact area.

The Hertzian model allows a simple definition of the contact force with a fairly good performance, for any contact interaction. However, it doesn't consider any energy dissipation phenomena, which is inconsistent from a physical point of view. For this reason, a great number of models that deal with this issue have been developed.

One of the most used constitutive laws is the one proposed by Lankarani and Nikravesh, with multiple applications [9]

$$F_N = K \cdot \delta^{3/2} + \chi \cdot \delta^{3/2} \cdot \dot{\delta} = K \cdot \delta^{3/2} \cdot \left(1 + \frac{3 \cdot (1 - c_r^2)}{4} \cdot \frac{\dot{\delta}}{\dot{\delta}^{(-)}}\right) \tag{10}$$

where χ denotes the hysteresis damping factor, a measure of the energy dissipated throughout the contact process. c_r is the coefficient of restitution, whereas $\dot{\delta}^{(-)}$ is the initial normal velocity and $\dot{\delta}$ represents the normal contact velocity. This model has proved to work well with contact events in which the value of c_r is close to unity and the impact velocities are low. Impacts at velocities higher than the wave propagation velocity have an energy dissipation mechanism not considered in this model, mainly in form of permanent deformation.

Another, more recent model is the one described by Flores et al., who considered the relation between the energy dissipated and the coefficient of restitution through the kinetic energy balance and the principle of conservation of momentum, the elastic strain energy stored due to the normal-force work and the energy dissipated due to internal damping to develop a constitutive law that can be applied to the entire range of values of c_r

$$F_N = K \cdot \delta^{3/2} + \chi \cdot \delta^{3/2} \cdot \dot{\delta} = K \cdot \delta^{3/2} \cdot \left(1 + \frac{8 \cdot (1 - c_r)}{5 \cdot c_r} \cdot \frac{\dot{\delta}}{\dot{\delta}^{(-)}}\right) \tag{11}$$

These two last models include in their definitions the relative contact velocities and the coefficient of restitution. However, the main problem is that they only consider two bodies in their conception, so, when dealing with contact events in which more bodies are involved, some unexpected and/or inconsistent results can be obtained. For example, in some cases, the value of the normal impact velocity could lead to attractive forces if three bodies collide successively, something that is possible. Some of these issues and are presented in the following sections.

3. FIRST MODEL: A BALL BEARING

The first model presented is a classical ball bearing, as shown in Figure 4(a). One of the most typical causes of failure in rotary machine is the appearance of defects in bearings [14]. According to some reports, almost half of the failures of electric motors have their origin in bearing-related breakdowns [15]. This kind of failure can lead to more severe problems in other parts of the engine, increasing dramatically the financial losses. Traditional maintenance methods consist of replacing the bearing periodically once a certain operation time expires. Two issues are associated to these methods: this way of proceeding is experience-based, which cannot consider factors such

https://doi.org/10.3311/ECCOMASMBD2021-114

as a wrong assembling, poor lubrication, etc.; and the location of the machines, which may be not easily accessible (for example, offshore turbines). For these reasons, predictive maintenance techniques are quite useful to analyse these components with frequency-based studies, allowing engineers to determine accurately the condition of the bearing without a periodic replacement.

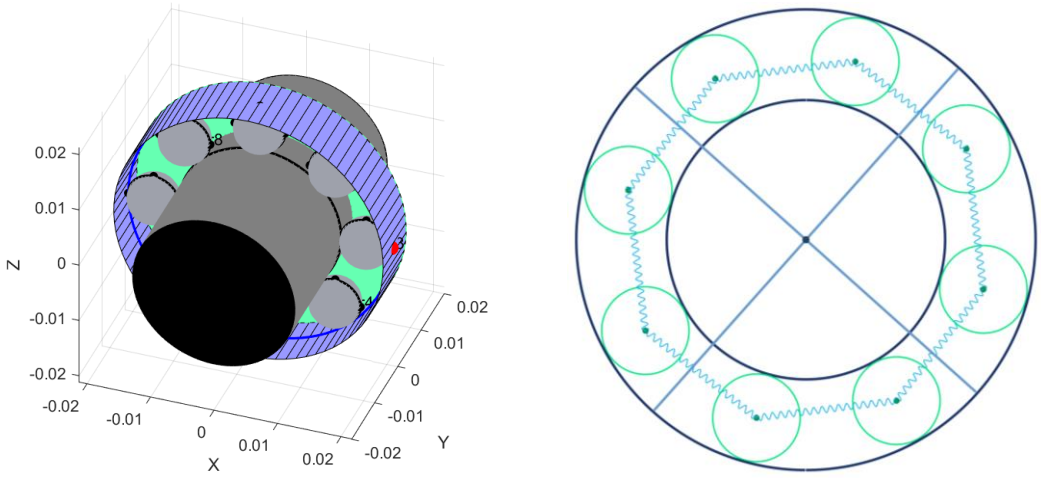

(a) (b)

Figure 4. Ball bearing model: (a) Matlab-generated animation of the first model; (b) Design of the bearing model, considering spring point-to-point elements to simulate the cage.

In this primitive model, the cage was modelled by a set of spring elements between the centres of the balls, as shown in Figure 4(b). The stiffness parameter of these spring elements was quite high, in order to keep the stability of the system but, at the same time, allowing them to vibrate properly. The inner race is a fixed body, so the model resembles to a real bearing tested in a machine bench, where the bearing is fixed to the shaft. The driving force is applied to the outer race, transmitting the motion through friction forces to the balls.

Two models were developed regarding contact interactions: the first one, based on the sphere-sphere contact interaction described above, neglecting any kind of axial loads, and the latter, more advanced, considering axial loads through a sphere-cylinder contact interaction. During the development of this contact algorithm, the main issue faced was the proper detection of the initial instant of contact. For the test model shown in Figure 5, in which a ball bounces along Z axis, for an elastic impact, the initial position should be reached after each impact.

Two Matlab integrators widely used were tested and compared. ODE45, which is based on the Runge-Kutta method developed by Dormand and Prince [16], stands out for being the most versatile Matlab integrator and being able to work reasonably well with almost all type of Initial Value Problems, thanks to its variable time step which allows an efficient computation. “45” makes reference to the order of formulas (4^{th} and 5^{th}) used by the algorithms. As can be seen in Figure 6, the values of the tolerances had a decisive impact on the results. *Abstol* denotes the absolute tolerance, a threshold value below which the value of the solution becomes unimportant. It determines the accuracy when the solution approaches zero. *Reltol*, and acronym for relative tolerance, is a measure of the error relative to the size of each solution component. It controls the number of correct digits in all solution components, except those smaller than threshold *AbsTol*. The main values for these two magnitudes are $1 \cdot 10^{-6}$ and $1 \cdot 10^{-3}$, respectively. For these, the results were a bit inconsistent, as the sphere gained energy after each rebound and surpassed the initial position at one point of the simulation. This issue was solved reducing these tolerances, first with an extreme value ($1 \cdot 10^{-12}$) and then looking for a balance between the accuracy of the results and the computational efficiency. The optimal values obtained for this model were $Abstol = 1 \cdot 10^{-6}$ and $Reltol = 1 \cdot 10^{-8}$, respectively. These provided consistent results, as the ball didn’t surpass the initial Z-axis position or lose energy after each impact either.

However, ODE45 integrator is not the Holy Grail and experiences some issues when dealing with stringent expensive tolerances, which arose when an inelastic impact was tested instead. In the case shown in Figure 7, the contact event was modelled with a coefficient of restitution of 0.7, using the Lankarani and Nikravesh model introduced earlier. As can be seen, the simulation collapses with ODE45, even for really small tolerance values.

https://doi.org/10.3311/ECCOMASMBD2021-114

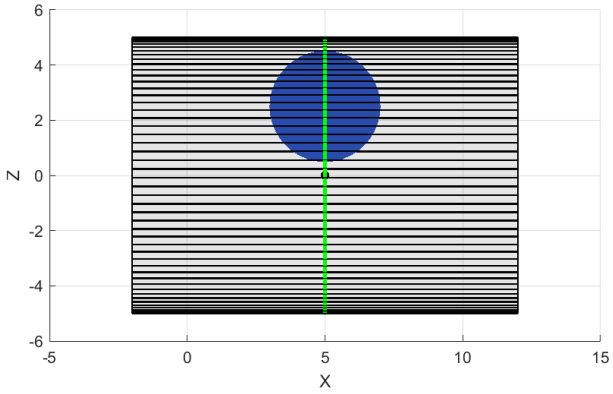

Figure 5. Matlab-generated animation of the sphere-cylinder interaction test model.

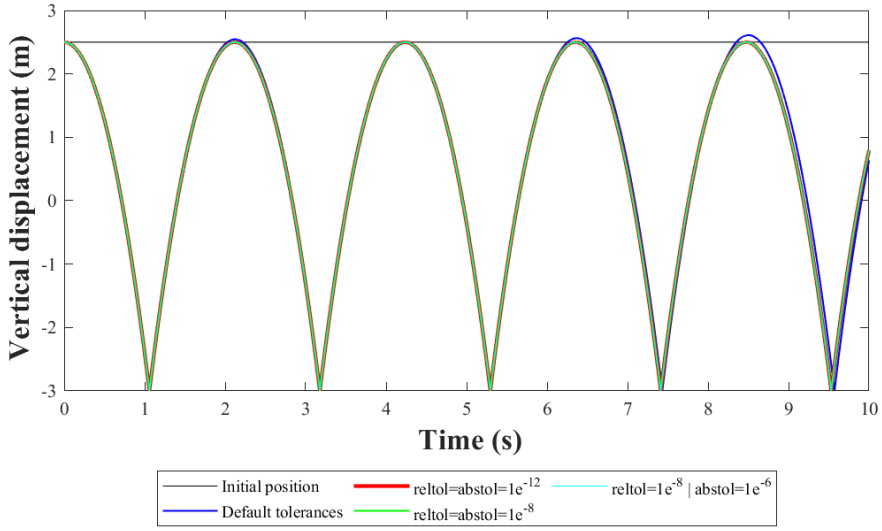

Figure 6. Variation in the results given by ODE45 Matlab integrator when changing the values of the tolerances associated to it.

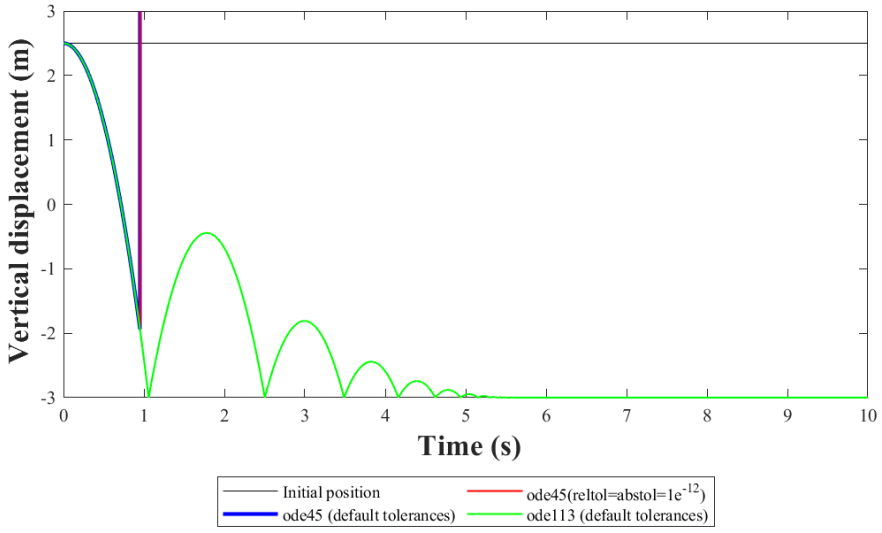

Figure 7. Evolution of the Z-axis position of the bouncing ball, for different values of time step, for a impact defined by a $c_r = 0.7$.

In contrast with this integrator, ODE113, which is a PECE implementation of Adams-Bashforth-Moulton methods [16], proved to give better results than ODE45, for a non-fully elastic impact. “113” makes reference to the fact that it is a variable order solver, from 1 to 13. PECE means Predict-Evaluate-Correct-Evaluate, where this second evaluation improves the accuracy of the method, as improved function values are used in the set of backpoints in the subsequent steps [17]. However, when testing the elastic impact (Hertzian model), this integrator led to a subsequent slight energy loss, preventing the ball from reaching the initial position.

https://doi.org/10.3311/ECCOMASMBD2021-114

Regarding the verification phase, the material properties of a ball bearing ER10K, presented in Table 1, were used. The PSD (Power Spectral Density) of the acceleration of the balls, for a healthy bearing, is shown in Figure 8. It can be observed a consistent behaviour of the model, as there is only a peak at low frequencies, caused by the own system, and there are no traces of defects.

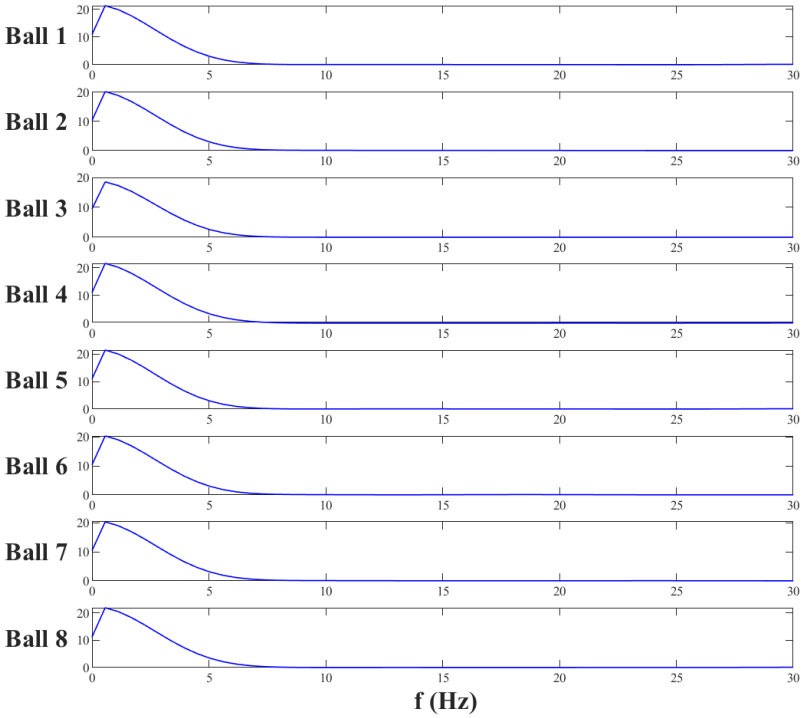

Figure 8. PSD of the acceleration of the balls generated by Matlab.

Table 1. Properties of the reference bearing (obtained from REXNORD catalog and experimental measures)

Property	Value
Shaft diameter / bore	15.875 mm
Outside diameter	47.000 mm
Mean diameter	31.438 mm
Number of balls	8
Ball diameter	7.938 mm
Contact angle	0º

4. SECOND MODEL: POOL/BILLIARD TABLE

The second model proposed was presented in a previous work [18] and has been now further developed, as can be seen in Figure 9. Pocket algorithm has been defined and implemented, so the balls fall when they get to them. Starting from the sphere-regular parallelepiped interaction introduced earlier, a sphere-triangular prism contact detection algorithm was developed for the ball-cushion interaction around the pockets. Each cushion was then divided into three bodies, as shown in Figure 10. The rounded area of the cushion in the cushions is at the moment being developed from the sphere-cylinder interaction presented above.

In this model, in which the balls can move freely in all directions, two different scenarios were considered: a permanent contact (between the balls and the cloth, as long as the ball is not hit so that it is lifted off the ground) and an intermittent one (between the balls themselves and these and the cushions). When calculating the value of both friction and contact forces, the peculiarities of each interaction had to be taken into account. The values of the parameters for each contact event were taken from experimental works [19]. Considering this, a Hertzian contact force was

https://doi.org/10.3311/ECCOMASMBD2021-114

chosen to calculate the value of normal force for the permanent contact, being the model proposed by Ambrósio the best choice to account for the friction force. On the other hand, for the ball-cushion interaction, which are not-fully elastic, the model defined by Lankarani and Nikravesh was the optimal option to obtain the value of the normal force, with Ambrósio's model characterising again the friction phenomena. Lastly, the contact events between the balls were modelled using again Lankarani and Nikravesh's model for the normal force and two different models for the friction force: Threlfall's approximation and a tangential velocity-dependent model developed by Alciatore [19]. The different values considered are shown in Table 2.

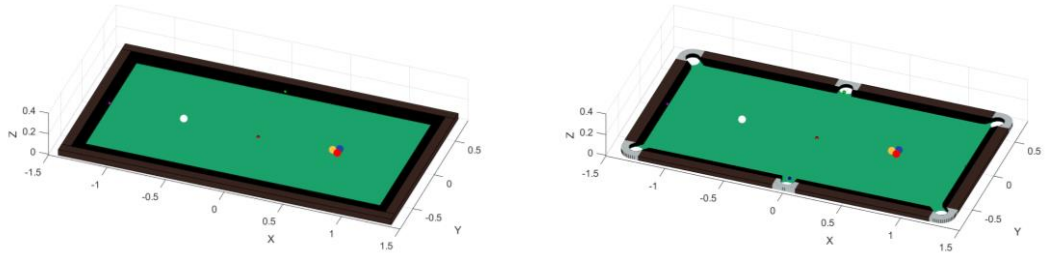

(a) (b)

Figure 9. Matlab-generated animation of the second model: (a) Previous version; (b) Current version.

Table 2. Restitution and friction coefficients used to model the different interactions of the system [19], [20].

Interaction	Contact force model	Friction force model	Friction coefficient	Restitution coefficient
Ball-ball	Lankarani and Nikravesh	Threlfall	0.06	0.93
		Alciatore	$9.951 \cdot 10^{-3} + 0.108 \cdot e^{-1.088 \cdot v}$	0.93
Ball-cloth	Hertz	Ambrósio	0.2	-
Ball-cushion	Lankarani and Nikravesh	-	-	0.85
		Ambrósio	0.14	0.98

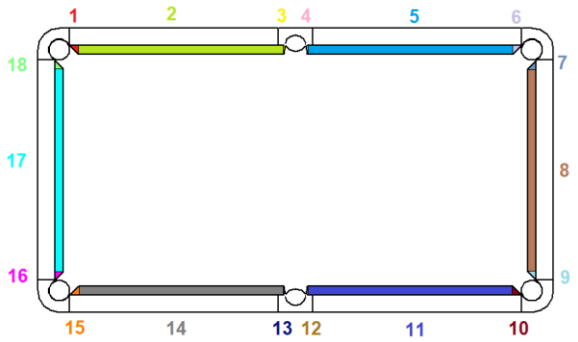

Figure 10. Arrangement of the bodies that form the cushions of the pool/billiard table.

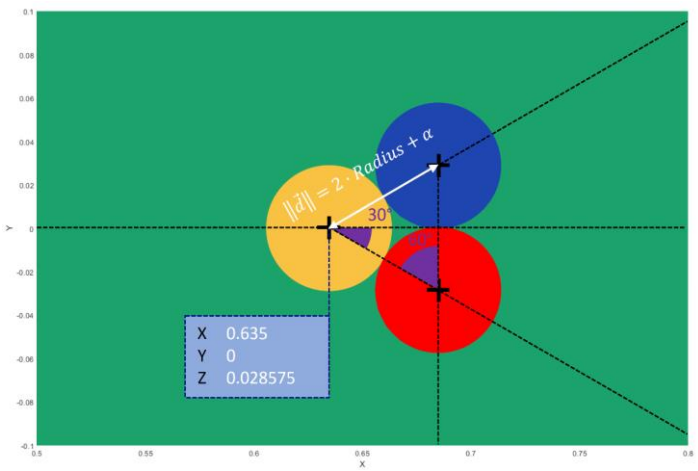

Figure 11. Arrangement of the balls as a function of α.

https://doi.org/10.3311/ECCOMASMBD2021-114

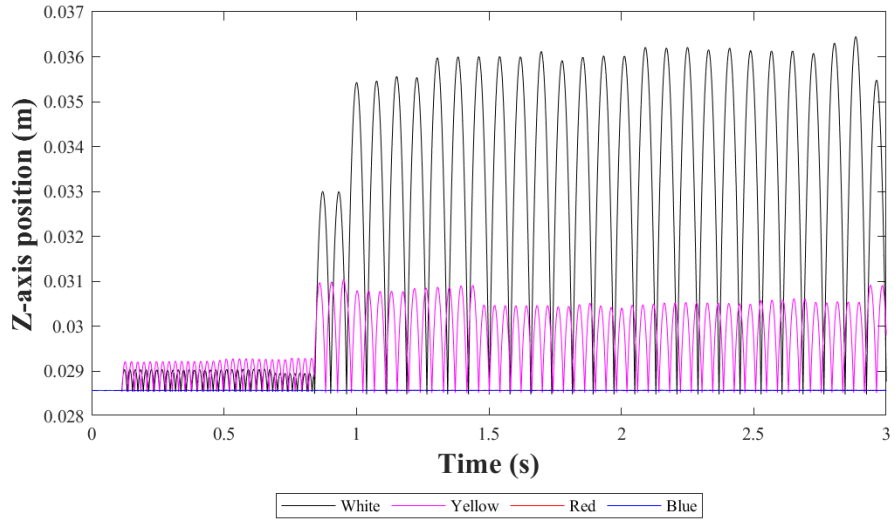

(a) $\alpha = 10^{-9}$ m

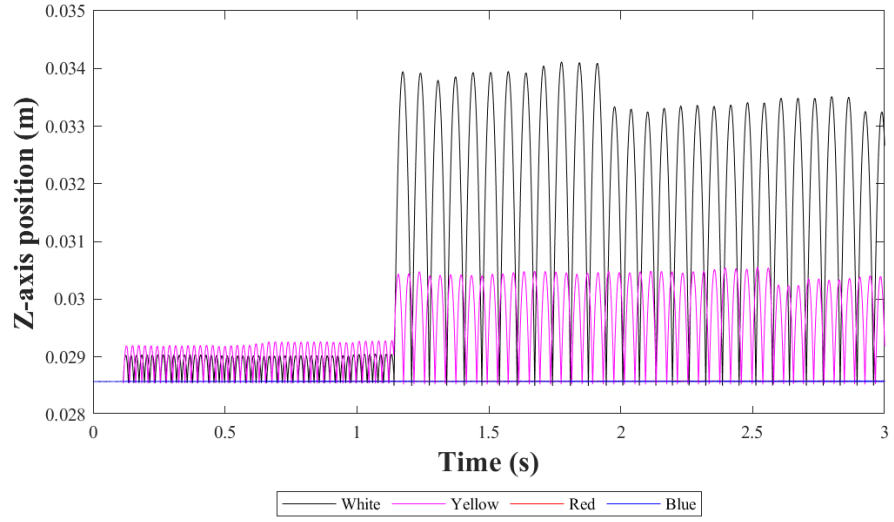

(b) $\alpha = 10^{-6}$ m

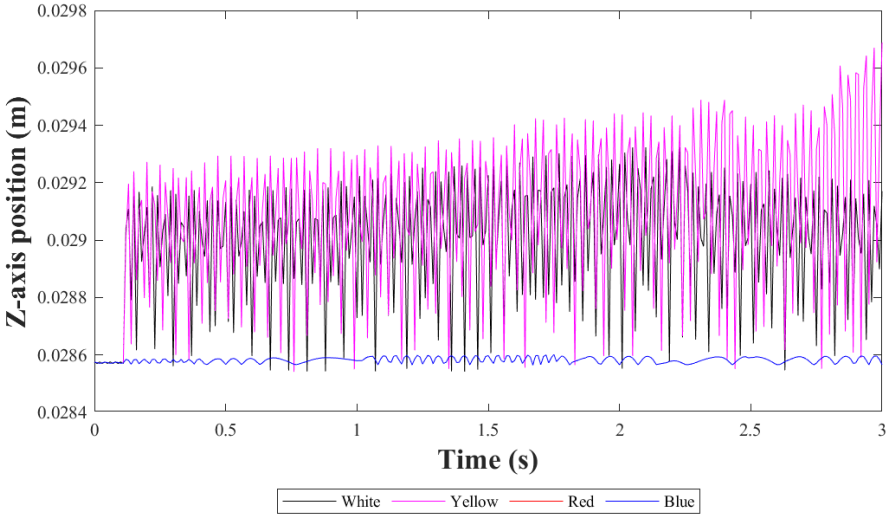

(c) $\alpha = 2.1325735 \cdot 10^{-4}$ m

Figure 12. Evolution of the Z-axis position components of the balls, depending on the value of α chosen.

In the early stages of the development of the model, balls static at the outset (coloured spheres in Figure 9) were arranged with a certain distance between their surfaces, avoiding the system to stall in excessively early times of the simulation due to the own definition of the forces. The coloured balls were always arranged so their mass centres formed an equilateral triangle. The distance between the mass centres of the coloured balls were defined by the expression $d = 2 \cdot \text{Radius} + \alpha$, being α a value set by the user, as shown in Figure 11. Several values were tested,

from the order of 10^{-9} to 10^{-4}. These proved to have a decisive impact on the results obtained. For instance, with lower values of α, some of the balls (mainly the cue and the yellow ones) tended to increase their position in global Z-axis as the analysis progressed and they rolled on the cloth (see Figure 12). As α was increased, the maximum values reached by these balls reduced, providing a more reasonable behaviour of the model, i.e., balls did not tend to gain energy and increase their Z-axis position. For the random value set of order 10^{-4}, the cue and yellow balls hardly moved in Z axis.

This is also an example of how a certain configuration of one of the contact interactions affects to the rest of contact events that happen simultaneously. For this reason, in the first simulations performed with this model during the tuning phase, both normal force in the ball-cloth contact and gravity force were neglected, therefore keeping constant Z-axis position. This resulted in a substantial reduction of the computing time, from an average of 15500 s for the lower values of α and 7700 s for the random value, to clearly lower values of 1730 s and 440 s, respectively. This modification of the model had some consequences: friction forces normal to the cloth had to be neglected to avoid the balls to either fly over the cloth or to sink into it.

5. THIRD MODEL: NEWTON'S CRADLE

The third model presented is a device widely used in educational contexts: Newton's cradle. This object is usually used to demonstrate the principles of conservation of momentum and conservation of energy through a set of swinging spheres (with the same size and mass) that collides elastically [21]. When a ball in one end of the chain is held at a certain height and released, so it collides with the remaining balls, the ball at the opposing end is kicked off and reaches about the same dropping height.

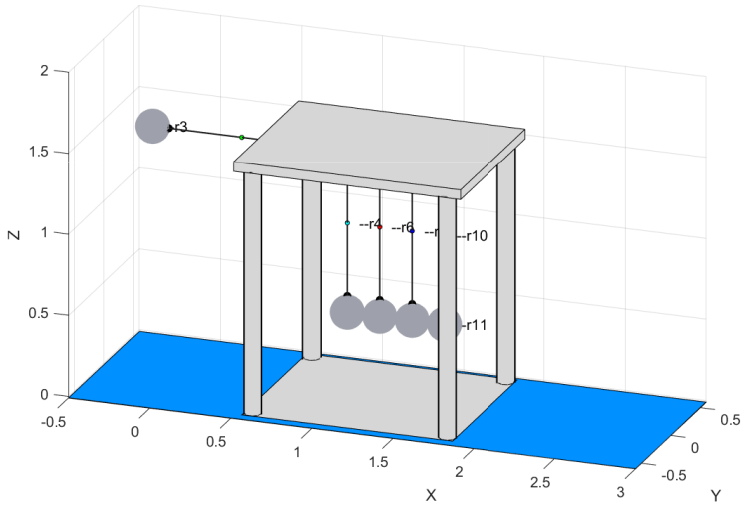

Figure 13. Matlab-generated animation of the third model.

The main assumptions in this model are usually to neglect friction phenomena and consider fully elastic contacts between the balls. In this case, the main issue that arose was the stall of the system when an inelastic contact (and, therefore, a contact model that considers explicitly normal relative velocity) was considered. Most dissipative contact force models, including the ones described above, include a ratio between the normal velocity at any given time and the value of the same magnitude at the initial instant of impact. If the bodies are together at that moment, which is the case of the static balls in Figure 13, these values will be the form of a 0/0 indeterminate form. A possible solution to this problem could be to consider a ratio of 1/1, but this is still under study.

Some data can be extracted from the graphs from Figure 14. The method based on standard Lagrange multipliers led to a failure of the system and, therefore, inconsistent results. Both Matlab integrators introduced earlier, ODE45 and ODE113, made the ball gain energy after each impact and reach a higher position, which is also incoherent. As in the previous model, reducing the default tolerances values improved the results, but also made the system lose some energy. Again, ODE113 provided better results at a lower computational cost, as the tolerance values were reduced to $1 \cdot 10^{-7}$, whereas ODE45 gave lower Z-axis positions for even lower tolerance values ($1 \cdot 10^{-10}$).

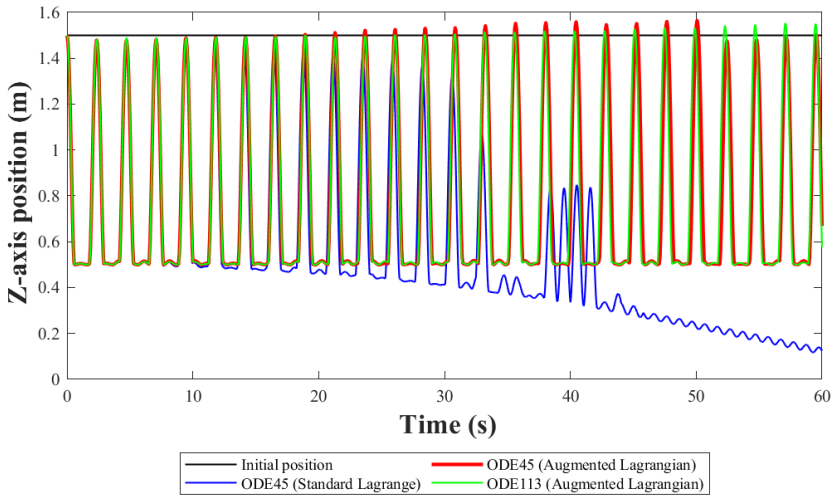

(a) Comparison between ODE45 and ODE113 Matlab integrators.

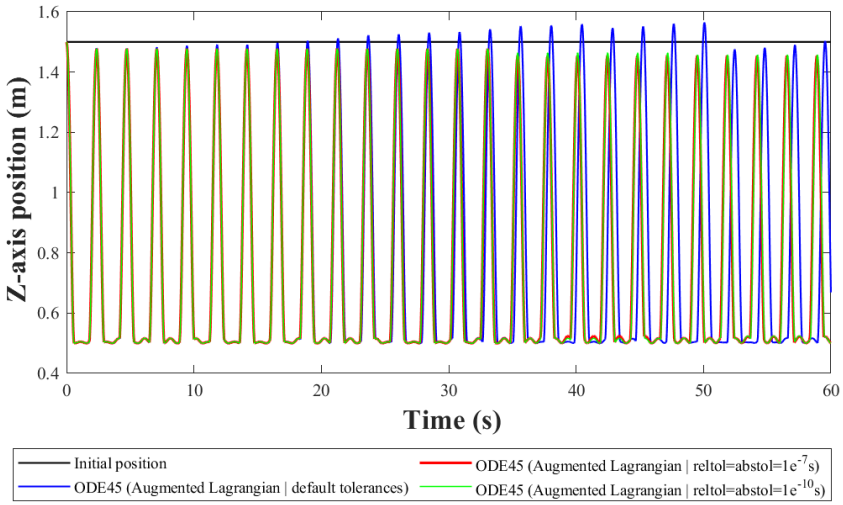

(b) Comparison for different tolerance values, for ODE45 integrator.

Figure 14. Evolution of Z-axis position of the ball released, throughout the simulation, for different settings of the integrators and constraint violation control methods.

6. CONCLUSIONS

Throughout this work, the main contact detection algorithms in the context of smooth multibody dynamics have been introduced and described. Some evolutions of these have been presented and applied to day-to-day systems and engineering applications, obtaining some promising results from each one of them, and facing some issues related to contact detection when performing dynamic analysis with Matlab software. Matlab default integrators proved to fall back when dealing with complex systems, specially when multiple contact/impact events take place simultaneously. Adjusting some parameters of these integrators improved considerably the results, but these settings involved a significant increase of the computational cost. However, there is still work to be made and some options that could be implemented, for example, a penetration-dependent integration scheme like the one some authors developed previously or to limit the number of iterations during each step.

ACKNOWLEDGMENTS

The authors would also like to acknowledge the support received by the Community of Madrid through its multi-year agreement with University Carlos III focused on its policy "Excelencia para el Profesorado Universitario".

REFERENCES

[1] J. Pagaimo, H. Magalhães, J. N. Costa, and J. Ambrósio, 'Derailment study of railway cargo vehicles

using a response surface methodology', *Veh. Syst. Dyn.*, 2020, doi: 10.1080/00423114.2020.1815810.

[2] M. Machado *et al.*, 'Development of a planar multibody model of the human knee joint', *Nonlinear Dyn.*, 2010, doi: 10.1007/s11071-009-9608-7.

[3] E. Corral, M. J. G. García, C. Castejon, J. Meneses, and R. Gismeros, 'Dynamic modeling of the dissipative contact and friction forces of a passive biped-walking robot', *Appl. Sci.*, 2020, doi: 10.3390/app10072342.

[4] G. Peláez, H. Rubio, E. Souto, and J. C. García-Prada, 'Optimal Model Reference Command Shaping for vibration reduction of Multibody-Multimode flexible systems: Initial Study.', in *Mechanisms and Machine Science*, 2019.

[5] R. Zander, M. Förg, and H. Ulbrich, 'Impacts on beam structures: Interactions of wave propagation and global dynamics', *Solid Mech. its Appl.*, vol. 1, pp. 327–338, 2007, doi: 10.1007/978-1-4020-5981-0_29.

[6] M. Filippini, M. Luke, I. Varfolomeev, D. Regazzi, and S. Beretta, 'Fatigue strength assessment of railway axles considering small-scale tests and damage calculations', *Procedia Struct. Integr.*, vol. 4, pp. 11–18, Jan. 2017, doi: 10.1016/J.PROSTR.2017.07.013.

[7] D. Infante-García, M. Marco, A. Zabala, F. Abbasi, E. Giner, and I. Llavori, 'On the role of contact and system stiffness in the measurement of principal variables in fretting wear testing', *Sensors (Switzerland)*, vol. 20, no. 15, pp. 1–20, Aug. 2020, doi: 10.3390/S20154152.

[8] M. Zamorano, M. J. Gómez Garcia, and C. Castejón, 'Selection of a mother wavelet as identification pattern for the detection of cracks in shafts', *J. Vib. Control*, p. 107754632110260, Jun. 2021, doi: 10.1177/10775463211026033.

[9] E. Corral, R. Gismeros Moreno, M. J. Gómez García, and C. Castejón, 'Nonlinear phenomena of contact in multibody systems dynamics: a review', *Nonlinear Dynamics*. Springer Science and Business Media B.V., pp. 1–27, Mar. 14, 2021, doi: 10.1007/s11071-021-06344-z.

[10] P. Flores and J. Ambrósio, 'On the contact detection for contact-impact analysis in multibody systems', *Multibody Syst. Dyn.*, 2010, doi: 10.1007/s11044-010-9209-8.

[11] E. Corral, R. Gismeros Moreno, J. Meneses, M. J. Gómez García, and C. Castejón, 'Spatial algorithms for geometric contact detection in multibody system dynamics', *Mathematics*, vol. 9, no. 12, Jun. 2021, doi: 10.3390/MATH9121359.

[12] M. Machado, P. Moreira, P. Flores, and H. M. Lankarani, 'Compliant contact force models in multibody dynamics: Evolution of the Hertz contact theory', *Mech. Mach. Theory*, 2012, doi: 10.1016/j.mechmachtheory.2012.02.010.

[13] M. Rodrigues da Silva, F. Marques, M. Tavares da Silva, and P. Flores, 'A compendium of contact force models inspired by Hunt and Crossley's cornerstone work', *Mech. Mach. Theory*, vol. 167, Jan. 2022, doi: 10.1016/J.MECHMACHTHEORY.2021.104501.

[14] J. E. Quiroga, G. Trujillo, and S. Quintero, 'Study on incipient fault bearing detection based on enveloping and cepstrum techniques', *Ingeniare*, vol. 20, no. 3, pp. 350–359, 2012, doi: 10.4067/S0718-33052012000300009.

[15] P. F. Albrecht, J. C. Appiarius, R. M. McCoy, E. L. Owen, and D. K. Sharma, 'Assessment of the reliability of motors in utility applications — updated', *IEEE Trans. Energy Convers.*, vol. EC-1, no. 1, pp. 39–46, 1986, doi: 10.1109/TEC.1986.4765668.

[16] L. F. Shampine and M. W. Reichelt, 'The MATLAB ode suite', *SIAM J. Sci. Comput.*, 1997, doi: 10.1137/S1064827594276424.

[17] M. M. Berry, 'A Variable-Step Double-Integration Multi-Step Integrator', Virginia Polytechnic Institute and State University, Blacksburg, Virginia, 2004.

[18] E. Corral, R. Gismeros, F. Marques, P. Flores, M. J. Gómez García, and C. Castejon, 'Dynamic Modeling and Analysis of Pool Balls Interaction', in *Computational Methods in Applied Sciences*, vol. 53, Springer, 2020, pp. 79–86.

[19] D. G. Alciatore, *The Illustrated Principles of Pool and Billiards*. Sterling Pub., 2004.

[20] S. Mathavan, M. R. Jackson, and R. M. Parkin, 'A theoretical analysis of billiard ball dynamics under cushion impacts', *Proc. Inst. Mech. Eng. Part C J. Mech. Eng. Sci.*, vol. 224, no. 9, pp. 1863–1873, Jan. 2010, doi: 10.1243/09544062JMES1964.

[21] N. A. De Sá Teixeira, A. M. Oliveira, and A. D. Silva, 'An information integration study on the intuitive physics of the Newton's cradle', *Psicologica*, vol. 35, no. 3, pp. 479–502, 2014.